
Unlocking Feature Visualization for Deeper Networks with **Magnitude Constrained Optimization**

Thomas Fel^{*1,2,4}, Thibaut Boissin^{*2,3}, Victor Boutin^{*1,2}, Agustín Picard^{*2,3}, Paul Novello^{*2,3},
Julien Colin^{1,5}, Drew Linsley¹, Tom Rousseau⁴, Rémi Cadène¹, Lore Goetschalckx¹,
Laurent Gardes⁴, Thomas Serre^{1,2}

¹Carney Institute for Brain Science, Brown University


²Artificial and Natural Intelligence Toulouse Institute

³Institut de Recherche Technologique Saint-Exupéry

⁴Innovation & Research Division, SNCF ⁵ELLIS Alicante, Spain.

{thomas_fel@brown.edu, thibaut.boissin@irt-saintexupery.com}

Abstract

Feature visualization has gained substantial popularity, particularly after the influential work by Olah et al. in 2017, which established it as a crucial tool for explainability. However, its widespread adoption has been limited due to a reliance on tricks to generate interpretable images, and corresponding challenges in scaling it to deeper neural networks. Here, we describe **MACO**, a simple approach to address these shortcomings. The main idea is to generate images by optimizing the phase spectrum while keeping the magnitude constant to ensure that generated explanations lie in the space of natural images. Our approach yields significantly better results – both qualitatively and quantitatively – and unlocks efficient and interpretable feature visualizations for large state-of-the-art neural networks. We also show that our approach exhibits an attribution mechanism allowing us to augment feature visualizations with spatial importance. We validate our method on a novel benchmark for comparing feature visualization methods, and release its visualizations for all classes of the ImageNet dataset on  [Lens](#).

Overall, our approach unlocks, for the first time, feature visualizations for large, state-of-the-art deep neural networks without resorting to any parametric prior image model.

1 Introduction

The field of Explainable Artificial Intelligence (XAI) [2, 3] has largely focused on characterizing computer vision models through the use of attribution methods [4–13]. These methods aim to explain the decision strategy of a network by assigning an importance score to each input pixel (or group of input pixels [14–16]), according to their contribution to the overall decision. Such approaches only offer a partial understanding of the learned decision processes as they aim to identify the location of the most discriminative features in an image, the “where”, leaving open the “what” question, *i.e.* the semantic meaning of those features. Recent work [17–22] has highlighted the intrinsic limitations of attribution methods [23–26], calling for the development of methods that provide a complementary explanation regarding the “what”.

Feature visualizations provide a bridge to fill this gap via the generation of images that elicit a strong response from specifically targeted neurons (or groups of neurons). One of the simplest approaches uses gradient ascent to search for such an image. In the absence of regularization, this optimization is

* The authors contributed equally.

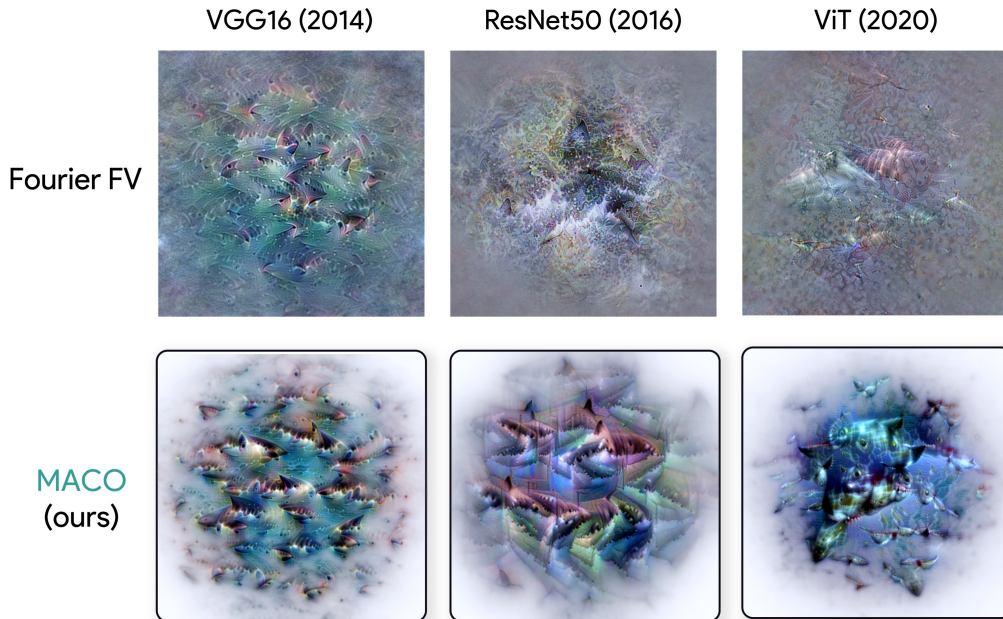


Figure 1: **Comparison between feature visualization methods for “White Shark” classification.** (Top) Standard Fourier preconditioning-based method for feature visualization [1]. (Bottom) Proposed approach, **MACO**, which incorporates a Fourier spectrum magnitude constraint.

known to yield highly noisy images – sometimes considered adversarial [27]. Hence, regularization methods are essential to rendering more acceptable candidate images. Such regularizations can consist of penalizing high frequencies in the Fourier domain [1, 28–31], regularizing the optimization process with data augmentation [1, 32–37] or restricting the search space to a subspace parameterized by a generative model [38–41]. The first two approaches provide faithful visualizations, as they only depend on the model under study; unfortunately, in practice, they still fail on large modern classification models (*e.g.*, ResNet50V2 [42] and ViT [43], see Figure 1). The third approach yields interpretable feature visualizations even for large models but at the cost of major biases: in that case, it is impossible to disentangle the true contributions of the model under study from those of the generative prior model. Herein, we introduce a new feature visualization approach that is applicable to the largest state-of-the-art networks without relying on any parametric prior image model.

Our proposed approach, called **M**agnitude **C**onstrained **O**ptimization (**MACO**), builds on the seminal work by Olah *et al.* who described the first method to optimize for maximally activating images in the Fourier space in order to penalize high-frequency content [1]. Our method is straightforward and essentially relies on exploiting the phase/magnitude decomposition of the Fourier spectrum, while exclusively optimizing the image’s phase while keeping its magnitude constant. Such a constraint is motivated by psychophysics experiments that have shown that humans are more sensitive to differences in phase than in magnitude [44–48]. Our contributions are threefold:

- (i) We unlock feature visualizations for large modern CNNs without resorting to any strong parametric image prior (see Figure 1).
- (ii) We describe how to leverage the gradients obtained throughout our optimization process to combine feature visualization with attribution methods, thereby explaining both “what” activates a neuron and “where” it is located in an image.
- (iii) We introduce new metrics to compare the feature visualizations produced with **MACO** to those generated with other methods.

As an application of our approach, we propose feature visualizations for FlexViT [49] and ViT [43] (logits and intermediate layers; see Figure 4). We also employ our approach on a feature inversion task to generate images that yield the same activations as target images to better understand what information is getting propagated through the network and which parts of the image are getting discarded by the model (on ViT, see Figure 6). Finally, we show how to combine our work with a state-of-the-art concept-based explainability method [50] (see Figure 6b). Much like feature

visualization, this method produces explanations on the semantic “what” that drives a model’s prediction by decomposing the latent space of the neural network into a series of “directions” – denoted concepts. More importantly, it also provides a way to locate each concept in the input image under study, thus unifying both axes – “what” and “where”. As feature visualization can be used to optimize in directions in the network’s representation space, we employ **MACO** to generate concept visualizations, thus allowing us to improve the human interpretability of concepts and reducing the risk of confirmation bias. We showcase these concept visualizations on an interactive website: **Lens**. The website allows browsing the most important concepts learned by a ResNet50 for all 1,000 classes of ImageNet [42].

2 Related Work

Feature visualization methods involve solving an optimization problem to find an input image that maximizes the activation of a target element (neuron, layer, or whole model) [10]. Most of the approaches developed in the field fall along a spectrum based on how strongly they regularize the model. At one end of the spectrum, if no regularization is used, the optimization process can search the whole image space, but this tends to produce noisy images and nonsensical high-frequency patterns [51].

To circumvent this issue, researchers have proposed to penalize high-frequency in the resulting images – either by reducing the variance between neighboring pixels [28], by imposing constraints on the image’s total variation [40, 41, 4], or by blurring the image at each optimization step [29]. However, in addition to rendering images of debatable validity, these approaches also suppress genuine, interesting high-frequency features, including edges. To mitigate this issue, a bilateral filter may be used instead of blurring, as it has been shown to preserve edges and improve the overall result [30]. Other studies have described a similar technique to decrease high frequencies by operating directly on the gradient, with the goal of preventing their accumulation in the resulting visualization [31]. One advantage of reducing high frequencies present in the gradient, as opposed to the visualization itself, is that it prevents high frequencies from being amplified by the optimizer while still allowing them to appear in the final image if consistently encouraged by the gradient. This process, known as “preconditioning” in optimization, can greatly simplify the optimization problem. The Fourier transform has been shown to be a successful preconditioner as it forces the optimization to be performed in a decorrelated and whitened image space [1]. The feature visualization technique we introduce in this work leverages a similar preconditioning. The emergence of high-frequency patterns in the absence of regularization is associated with a lack of robustness and sensitivity of the neural network to adversarial examples [27], and consequently, these patterns are less often observed in adversarially robust models [34, 33, 32]. An alternative strategy to promote robustness involves enforcing small perturbations, such as jittering, rotating, or scaling, in the visualization process [35], which, when combined with a frequency penalty [1], has been proved to greatly enhance the generated images.

Unfortunately, previous methods in the field of feature visualization have been limited in their ability to generate visualizations for newer architectures beyond VGG, resulting in a lack of interpretable visualizations for larger networks like ResNets [1]. Consequently, researchers have shifted their focus to approaches that leverage statistically learned priors to produce highly realistic visualizations. One such approach involves training a generator, like a GAN [40] or an autoencoder [52, 41], to map points from a latent space to realistic examples and optimizing within that space. Alternatively, a prior can be learned to provide the gradient (w.r.t the input) of the probability and optimize both the prior and the objective jointly [41, 30]. Another method involves approximating a generative model prior by penalizing the distance between output patches and the nearest patches retrieved from a database of image patches collected from the training data [38]. Although it is well-established that learning an image prior produces realistic visualizations, it is difficult to distinguish between the contributions of the generative models and that of the neural network under study. Hence, in this work, we focus on the development of visualization methods that rely on minimal priors to yield the least biased visualizations.

3 Magnitude-Constrained Feature Visualization

Notations Throughout, we consider a general supervised learning setting, with an input space $\mathcal{X} \subseteq \mathbb{R}^{h \times w}$, an output space $\mathcal{Y} \subseteq \mathbb{R}^c$, and a classifier $f : \mathcal{X} \rightarrow \mathcal{Y}$ that maps inputs $x \in \mathcal{X}$ to a prediction $y \in \mathcal{Y}$. Without loss of generality, we assume that f admits a series of L intermediate

spaces $\mathcal{A}_\ell \subseteq \mathbb{R}^{p_\ell}$, $1 < \ell < L$. In this setup, $f_\ell : \mathcal{X} \rightarrow \mathcal{A}_\ell$ maps an input to an intermediate activation $\mathbf{v} = (v_1, \dots, v_{p_\ell})^\top \in \mathcal{A}_\ell$ of f . We respectively denote \mathcal{F} and \mathcal{F}^{-1} as the 2-D Discrete Fourier Transform (DFT) on \mathcal{X} and its inverse.

Optimization Criterion. The primary goal of a feature visualization method is to produce an image \mathbf{x}^* that maximizes a given criterion $\mathcal{L}_v(\mathbf{x}) \in \mathbb{R}$; usually some value aggregated over a subset of weights in a neural network f (neurons, channels, layers, logits). A concrete example consists in finding a natural "prototypical" image \mathbf{x}^* of a class $k \in \llbracket 1, K \rrbracket$ without using a dataset or generative models. However, optimizing in the pixel space $\mathbb{R}^{W \times H}$ is known to produce noisy, adversarial-like \mathbf{x}^* (see section 2). Therefore, the optimization is constrained using a regularizer $\mathcal{R} : \mathcal{X} \rightarrow \mathbb{R}^+$ to penalize unrealistic images:

$$\mathbf{x}^* = \arg \max_{\mathbf{x} \in \mathcal{X}} \mathcal{L}_v(\mathbf{x}) - \lambda \mathcal{R}(\mathbf{x}). \quad (1)$$

In Eq. 1, λ is a hyperparameter used to balance the main optimization criterion \mathcal{L}_v and the regularizer \mathcal{R} . Finding a regularizer that perfectly matches the structure of natural images is hard, so proxies have to be used instead. Previous studies have explored various forms of regularization spanning from total variation, ℓ_1 , or ℓ_2 loss [40, 41, 4]. More successful attempts rely on the reparametrization of the optimization problem in the Fourier domain rather than on regularization.

3.1 A Fourier perspective

Mordvintsev *et al.* [53] noted in their seminal work that one could use differentiable image parametrizations to facilitate the maximization of \mathcal{L}_v . Olah *et al.* [1] proposed to reparametrize the images using their Fourier spectrum. Such a parametrization allows amplifying the low frequencies using a scalar \mathbf{w} . Formally, the prototypical image \mathbf{x}^* can be written as $\mathbf{x}^* = \mathcal{F}^{-1}(z^* \odot \mathbf{w})$ with $z^* = \arg \max_{z \in \mathbb{C}^{W \times H}} \mathcal{L}_v(\mathcal{F}^{-1}(z \odot \mathbf{w}))$. Finding \mathbf{x}^* boils down to optimizing a Fourier buffer $z = \mathbf{a} + i\mathbf{b}$ together with boosting the low-frequency components and then recovering the final image by inverting the optimized Fourier buffer using inverse Fourier transform.

However, multiple studies have shown that the resulting images are not sufficiently robust, in the sense that a small change in the image can cause the criterion \mathcal{L}_v to drop. Therefore, it is common to see robustness transformations applied to candidate images throughout the optimization process. In other words, the goal is to ensure that the generated image satisfies the criterion even if it is rotated by a few degrees or jittered by a few pixels. Formally, given a set of possible transformation functions – sometimes called augmentations – that we denote \mathcal{T} such that for any transformation $\tau \sim \mathcal{T}$, we have $\tau(\mathbf{x}) \in \mathcal{X}$, the optimization becomes $z^* = \arg \max_{z \in \mathbb{C}^{W \times H}} \mathbb{E}_{\tau \sim \mathcal{T}} (\mathcal{L}_v((\tau \circ \mathcal{F}^{-1})(z \odot \mathbf{w}))$.

Empirically, it is common knowledge that the deeper the models are, the more transformations are needed and the greater their magnitudes should be. To make their approach work on models like VGG, Olah *et al.* [1] used no less than a dozen transformations. However, this method fails for modern architectures, no matter how many transformations are applied. We argue that this may come from the low-frequency scalar (or booster) no longer working with models that are too deep. For such models, high frequencies eventually come through, polluting the resulting images with high-frequency content – making them impossible to interpret by humans. To empirically illustrate this phenomenon, we compute the k logit visualizations obtained by maximizing each of the logits corresponding to the k classes of a ViT using the parameterization used by Olah *et al.* In Figure 2 (left), we show the average of the

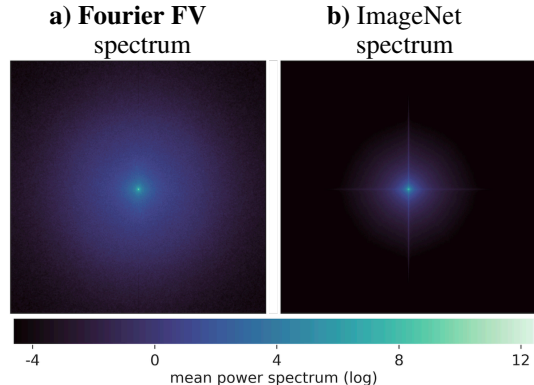


Figure 2: **Comparison between Fourier FV and natural image power spectrum.** In (a), the power spectrum is averaged over 10 different logits visualizations for each of the 1000 classes of ImageNet. The visualizations are obtained using the **Fourier FV** method to maximize the logits of a ViT network [1]. In (b) the spectrum is averaged over all training images of the ImageNet dataset.

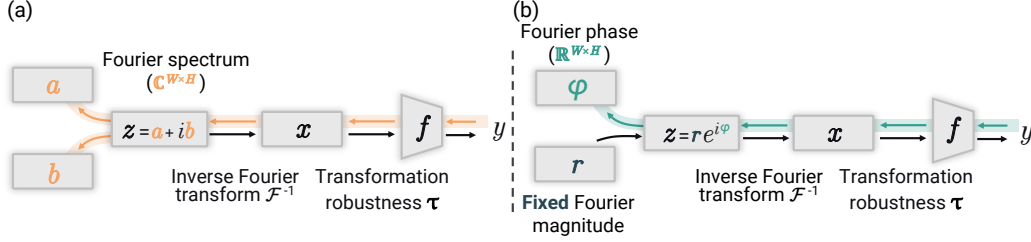


Figure 3: **Overview of the approach:** (a) Current Fourier parameterization approaches optimize the entire spectrum (yellow arrow). (b) In contrast, the optimization flow in our approach (green arrows) goes from the network activation (y) to the phase of the spectrum (ϕ) of the input image (x).

spectrum of these generated visualizations over all classes: $\frac{1}{k} \sum_{i=1}^k |\mathcal{F}(x_i^*)|$. We compare it with the average spectrum of images on the ImageNet dataset (denoted \mathcal{D}): $\mathbb{E}_{x \sim \mathcal{D}}(|\mathcal{F}(x)|)$ (Figure 2, right panel). We observe that the images obtained through optimization put much more energy into high frequencies compared to natural images. Note that we did not observe this phenomenon in older models such as LeNet or VGG.

In the following section, we introduce our method named **MACO**, which is motivated by this observation. We constrain the magnitude of the visualization to a natural value, enabling natural visualization for any contemporary model, and reducing the number of required transformations to only two.

3.2 MACO: from Regularization to Constraint

Parameterizing the image in the Fourier space makes it possible to directly manipulate the image in the frequency domain. We propose to take a step further and decompose the Fourier spectrum z into its polar form $z = r e^{i\phi}$ instead of its cartesian form $z = a + ib$, which allows us to disentangle the magnitude (r) and the phase (ϕ).

It is known that human recognition of objects in images is driven not by magnitude but by phase [44–48]. Motivated by this, we propose to optimize the phase of the Fourier spectrum while fixing its magnitude to a typical value of a natural image (with few high frequencies). In particular, the magnitude is kept constant at the average magnitude computed over a set of natural images (such as ImageNet), so $r = \mathbb{E}_{x \sim \mathcal{D}}(|\mathcal{F}(x)|)$. Note that this spectrum needs to be calculated only once and can be used at will for other tasks.

Therefore, our method does not backpropagate through the entire Fourier spectrum but only through the phase (Figure 3), thus reducing the number of parameters to optimize by half. Since the magnitude of our spectrum is constrained, we no longer need hyperparameters such as λ or scaling factors, and the generated image at each step is naturally plausible in the frequency domain. We also enhance the quality of our visualizations via two data augmentations: random crop and additive uniform noise. To the best of our knowledge, our approach is the first to completely alleviate the need for explicit regularization – using instead a hard constraint on the solution of the optimization problem for feature visualization. To summarize, we formally introduce our method:

Definition 3.1 (MACO). *The feature visualization results from optimizing the parameter vector ϕ such that:*

$$\phi^* = \arg \max_{\phi \in \mathbb{R}^{W \times H}} \mathbb{E}_{\tau \sim \mathcal{T}} (\mathcal{L}_v((\tau \circ \mathcal{F}^{-1})(r e^{i\phi})) \text{ where } r = \mathbb{E}_{x \sim \mathcal{D}}(|\mathcal{F}(x)|)$$

The feature visualization is then obtained by applying the inverse Fourier transform to the optimal complex-valued spectrum: $x^ = \mathcal{F}^{-1}(r e^{i\phi^*})$*

Transparency for free: Visualizations often suffer from repeated patterns or unimportant elements in the generated images. This can lead to readability problems or confirmation biases [54]. It is

Algorithm 1 MACO

Require: $r, \phi_0 \sim \mathcal{U}([- \pi, \pi])^{W \times H}$

Require: $\alpha = 0$

for $n \in \llbracket 0, N \rrbracket$ **do**

$\tau = \text{sample}(\mathcal{T})$

$x_n = (\tau \circ \mathcal{F}^{-1})(r e^{i\phi_n})$

$\phi_{n+1} = \phi_n + \eta \nabla_{\phi} \mathcal{L}_v(x_n)$

$\alpha = \alpha + |\nabla_{x_n} \mathcal{L}_v(x_n)|$

end for

return $x^* = \mathcal{F}^{-1}(r e^{i\phi_N}), \alpha$

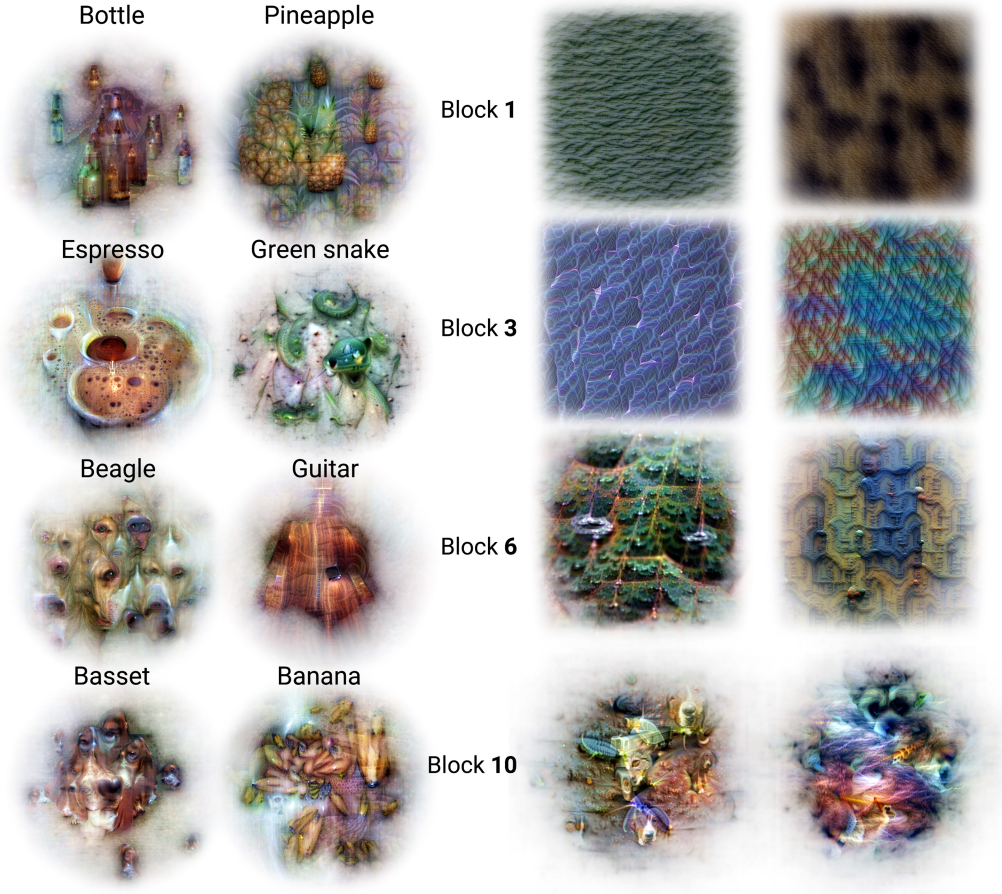


Figure 4: **(left) Logits and (right) internal representations of FlexViT.** **MACO** was used to maximize the activations of **(left)** logit units and **(right)** specific channels located in different blocks of the FlexViT (blocks 1, 2, 6 and 10 from left to right).

important to ensure that the user is looking at what is truly important in the feature visualization. The concept of transparency, introduced in [53], addresses this issue but induces additional implementation efforts and computational costs.

We propose an effective approach, which leverages attribution methods, that yields a transparency map α for the associated feature visualization without any additional cost. Our solution shares theoretical similarities with SmoothGrad [5] and takes advantage of the fact that during backpropagation, we can obtain the intermediate gradients on the input $\partial\mathcal{L}_v(\mathbf{x})/\partial\mathbf{x}$ for free as $\frac{\partial\mathcal{L}_v(\mathbf{x})}{\partial\varphi} = \frac{\partial\mathcal{L}_v(\mathbf{x})}{\partial\mathbf{x}} \frac{\partial\mathbf{x}}{\partial\varphi}$. We store these gradients throughout the optimization process and then average them, as done in SmoothGrad, to identify the areas that have been modified/attended to by the model the most during the optimization process. We note that a similar technique has recently been used to explain diffusion models [55]. In Algorithm 1, we provide pseudo-code for **MACO** and an example of the transparency maps in Figure 6 (third column).

4 Evaluation

We now describe and compute three different scores to compare the different feature visualization methods: Fourier (Olah *et al.*), CBR (optimization in the pixel space), and **MACO** (ours). It is important to note that these scores are only applicable to output logit visualizations. To keep a fair comparison, we restrict the benchmark to methods that do not rely on any learned image priors. Indeed, methods with learned prior will inevitably yield lower FID scores (and lower plausibility score) as the prior forces the generated visualizations to lie on the manifold of natural images.

Plausibility score. We consider a feature visualization plausible when it is similar to the distribution of images belonging to the class it represents. We quantify the plausibility through an OOD metric (Deep-KNN, recently used in [56]): it measures how far a feature visualization deviates from the corresponding ImageNet object category images based on their representation in the network’s intermediate layers (see Table 1).

FID score. The FID quantifies the similarity between the distribution of the feature visualizations and that of natural images for the same object category. Importantly, the FID measures the distance between two distributions, while the plausibility score quantifies the distance from a sample to a distribution. To compute the FID, we used images from the ImageNet validation set and used the Inception v3 last layer (see Table 1). Additionally, we center-cropped our 512×512 images to 299×299 images to avoid the center-bias problem [39].

Transferability score. This score measures how consistent the feature visualizations are with other pre-trained classifiers. To compute the transferability score, we feed the obtained feature visualizations into 6 additional pre-trained classifiers (MobileNet [57], VGG16 [58], Xception [59], EfficientNet [60], Tiny ConvNext [61] and Densenet [62]), and we report their classification accuracy (see Table 2).

All scores are computed using 500 feature visualizations, each of them maximizing the logit of one of the ImageNet classes obtained on the FlexiViT [49], ViT[63], and ResNetV2[64] models. For the feature visualizations derived from Olah *et al.* [1], we used all 10 transformations set from the Lucid library*. CBR denotes an optimization in pixel space and using the same 10 transformations, as described in [29]. For **MACO**, τ only consists of two transformations; first we add uniform noise $\delta \sim \mathcal{U}([-0.1, 0.1])^{W \times H}$ and crops and resized the image with a crop size drawn from the normal distribution $\mathcal{N}(0.25, 0.1)$, which corresponds on average to 25% of the image. We used the NAdam optimizer [65] with $lr = 1.0$ and $N = 256$ optimization steps. Finally, we used the implementation of [1] and CBR which are available in the Xplique library [66] † which is based on Lucid.

	FlexiViT	ViT	ResNetV2		FlexiViT	ViT	ResNetV2
• Plausibility score (1-KNN) (↓)				• Transferability score (↑): MACO / Fourier [1]			
MACO	1473	1097	1248	MobileNet	68 / 38	48 / 37	93 / 36
Fourier [1]	1815	1817	1837	VGG16	64 / 30	50 / 30	90 / 20
CBR [29]	1866	1920	1933	Xception	85 / 61	73 / 62	97 / 64
• FID Score (↓)				Eff. Net	88 / 25	63 / 25	82 / 21
MACO	230.68	241.68	312.66	ConvNext	96 / 52	84 / 55	93 / 60
Fourier [1]	250.25	257.81	318.15	DenseNet	84 / 32	66 / 31	93 / 25
CBR [29]	247.12	268.59	346.41				

Table 1: Plausibility and FID scores for different feature visualization methods applied on FlexiViT, ViT and ResNetV2

Table 2: Transferability scores for different feature visualization methods applied on FlexiViT, ViT and ResNetV2.

For all tested metrics, we observe that **MACO** produces better feature visualizations than those generated by Olah *et al.* [1] and CBR [29]. We would like to emphasize that our proposed evaluation scores represent the first attempt to provide a systematic evaluation of feature visualization methods, but we acknowledge that each individual metric on its own is insufficient and cannot provide a comprehensive assessment of a method’s performance. However, when taken together, the three proposed scores provide a more complete and accurate evaluation of the feature visualization methods.

4.1 Human psychophysics study

Ultimately, the goal of any feature visualization method is to demystify the CNN’s underlying decision process in the eyes of human users. To evaluate **MACO**’s ability to do this, we closely followed the psychophysical paradigm introduced in [67]. In this paradigm, the participants are presented with examples of a model’s “favorite” inputs (i.e., feature visualization generated for a given unit) in addition to two query inputs. Both queries represent the same natural image, but have a

*<https://github.com/tensorflow/lucid>

†<https://github.com/deel-ai/xplique>

FlexiViT	Plausibility (\downarrow)	FID (\downarrow)	logit magnitude (\uparrow)
MACO	571.68	211.0	5.12
- transparency	617.9 (+46.2)	208.1 (-2.9)	5.05 (-0.1)
- crop	680.1 (+62.2)	299.2 (-91.1)	8.18 (+3.1)
- noise	707.3 (+27.1)	324.5 (-25.3)	11.7 (+3.5)
Fourier [1]	673.3	259.0	3.22
- augmentations	735.9 (+62.6)	312.5 (+53.5)	12.4 (+9.2)

Table 3: **Ablation study on the FlexiViT model:** This reveals that 1. augmentations help to have better FID and Plausibility scores, but lead to lesser salients visualizations (softmax value), 2. Fourier [1] benefits less from augmentations than **MACO**.

different part of the image hidden from the model by a square occludor. The task for participants is to judge which of the two queries would be “favored by the model” (i.e., maximally activate the unit). The rationale here is that a good feature visualization method would enable participants to more accurately predict the model’s behavior. Here, we compared four visualization conditions (manipulated between subjects): Olah [1], **MACO** with the transparency mask (the transparency mask is described in 3.2), **MACO** without the transparency mask, and a control condition in which no visualizations were provided. In addition, the network (VGG16, ResNet50, ViT) was a within-subject variable. The units to be understood were taken from the output layer.

Based on the data of 174 participants on Prolific (www.prolific.com) [September 2023], we found both visualization and network to significantly predict the logodds of choosing the right query (Fig. 5). That is, the logodds were significantly higher for participants in both the **MACO** conditions compared to Olah. On the other hand, our tests did not yield a significant difference between Olah and the control condition, or between the two **MACO** conditions. Finally, we found that, overall, ViT was significantly harder to interpret than ResNet50 and VGG16, with no significant difference observed between the latter two networks. Full experiment and analysis details can be found in the supplementary materials, section C. Taken together, these results support our claim that even if feature visualization methods struggle in offering interpretable information as networks scale, **MACO** still convincingly helps people better understand deeper models while Olah’s method [1] does not.

4.2 Ablation study

To disentangle the effects of the various components of **MACO**, we perform an ablation study on the feature visualization applications. We consider the following components: (1) the use of a magnitude constraint, (2) the use of the random crop, (3) the use of the noise addition, and (4) the use of the transparency mask. We perform the ablation study on the FlexiViT model, and the results are presented in Table 3. We observe an inherent tradeoff between optimization quality (measured by logit magnitude) on one side, and the plausibility (and FID) scores on the other side. This reveals that plausible images which are close to the natural image distribution do not necessarily maximize the logit. Finally, we observe that the transparency mask does not significantly affect any of the scores confirming that it is mainly a post-processing step that does not affect the feature visualization itself.

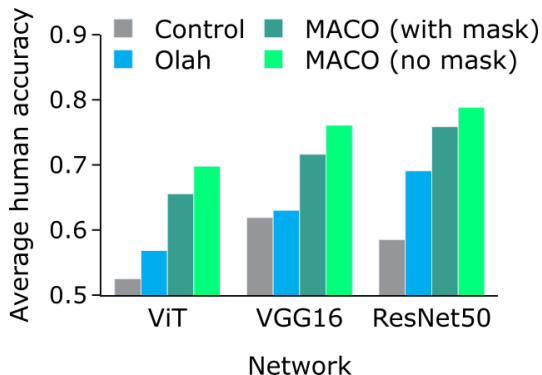


Figure 5: **Human causal understanding of model activations.** We follow the experimental procedure introduced in [67] to evaluate Olah and **MACO** visualizations on 3 different networks. The control condition is when the participant did not see any feature visualization.

5 Applications

We demonstrate the versatility of the proposed **MACO** technique by applying it to three different XAI applications:

Logit and internal state visualization. For logit visualization, the optimization objective is to maximize the activation of a specific unit in the logits vector of a pre-trained neural network (here a FlexiViT[49]). The resulting visualizations provide insights into the features that contribute the most to a class prediction (refer to Figure 4a). For internal state visualization, the optimization objective is to maximize the activation of specific channels located in various intermediate blocks of the network (refer to Figure 4b). This visualization allows us to better understand the kind of features these blocks – of a FlexiViT[49] in the figure – are sensitive to.

Feature inversion. The goal of this application is to find an image that produces an activation pattern similar to that of a reference image. By maximizing the similarity to reference activations, we are able to generate images representing the same semantic information at the target layer but without the parts of the original image that were discarded in the previous stages of the network, which allows us to better understand how the model operates. Figure 6a displays the images (second column) that match the activation pattern of the penultimate layer of a ViT when given the images from the first column. We also provide examples of transparency masks based on attribution (third column), which we apply to the feature visualizations to enhance them (fourth column).

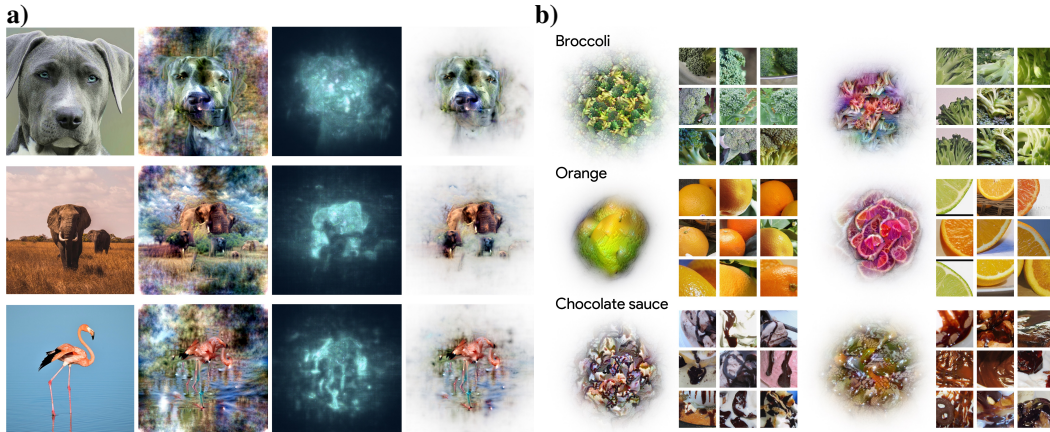


Figure 6: **Feature inversion and concept visualization.** **a)** Images in the second column match the activation pattern of the penultimate layer of a ViT when fed with the images of the first column. In the third column, we show their corresponding attribution-based transparency masks, leading to better feature visualization when applied (fourth column). **b)** **MACO** is used to visualize concept vectors extracted with the CRAFT method [50]. The concepts are extracted from a ResNet50 trained on ImageNet. All visualizations for all ImageNet classes are available at [Lens](#).

Concept visualization. Herein we combine **MACO** with concept-based explainability. Such methods aim to increase the interpretability of activation patterns by decomposing them into a set of concepts [68]. In this work, we leverage the CRAFT concept-based explainability method [50], which uses Non-negative Matrix Factorization to decompose activation patterns into main directions – that are called concepts –, and then, we apply **MACO** to visualize these concepts in the pixel space. To do so, we optimize the visualization such that it matches the concept activation patterns. In Figure 6b, we present the top 2 most important concepts (one concept per column) for five different object categories (one category per row) in a ResNet50 trained on ImageNet. The concepts’ visualizations are followed by a mosaic of patches extracted from natural images: the patches that maximally activate the corresponding concept.

6 Limitations

We have demonstrated the generation of realistic explanations for large neural networks by imposing constraints on the magnitude of the spectrum. However, it is important to note that generating realistic images does not necessarily imply effective explanation of the neural networks. The metrics introduced in this paper allow us to claim that our generated images are closer to natural images in latent space, that our feature visualizations are more plausible and better reflect the original distribution. However, they do not necessarily indicate that these visualizations help humans in effectively communicating with the models or conveying information easily to humans. Furthermore, in order for a feature visualization to provide informative insights about the model, including spurious features, it may need to generate visualizations that deviate from the spectrum of natural images. Consequently, these visualizations might yield lower scores using our proposed metrics. Simultaneously, several interesting studies have highlighted the weaknesses and limitations of feature visualizations [54, 69, 67]. One prominent criticism is their lack of interpretability for humans, with research demonstrating that dataset examples are more useful than feature visualizations in understanding convolutional neural networks (CNNs) [54]. This can be attributed to the lack of realism in feature visualizations and their isolated use as an explainability technique. With our approach, **MACO**, we take an initial step towards addressing this limitation by introducing magnitude constraints, which lead to qualitative and quantitative improvements. Additionally, through our website, we promote the use of feature visualizations as a supportive and complementary tool alongside other methods such as concept-based explainability, exemplified by CRAFT [50]. We emphasize the importance of feature visualizations in combating confirmation bias and encourage their integration within a comprehensive explainability framework.

7 Conclusions

In this paper, we introduced a novel approach, **MACO**, for efficiently generating feature visualizations in modern deep neural networks based on (i) a hard constraint on the magnitude of the spectrum to ensure that the generated visualizations lie in the space of natural images, and (ii) a new attribution-based transparency mask to augment these feature visualizations with the notion of spatial importance. This enhancement allowed us to scale up and unlock feature visualizations on large modern CNNs and vision transformers without the need for strong – and possibly misleading – parametric priors. We also complement our method with a set of three metrics to assess the quality of the visualizations. Combining their insights offers a way to compare the techniques developed in this branch of XAI more objectively. We illustrated the scalability of **MACO** with feature visualizations of large models like ViT, but also feature inversion and concept visualization. Lastly, by improving the realism of the generated images without using an auxiliary generative model, we supply the field of XAI with a reliable tool for explaining the semantic (“what” information) of modern vision models.

Acknowledgments

This work was conducted as part the DEEL[‡] project. It was funded by ONR grant (N00014-19-1-2029), NSF grant (IIS-1912280 and EAR-1925481), and the Artificial and Natural Intelligence Toulouse Institute (ANITI) grant #ANR19-PI3A-0004. The computing hardware was supported in part by NIH Office of the Director grant #S10OD025181 via the Center for Computation and Visualization (CCV) at Brown University. J.C. has been partially supported by Intel Corporation, a grant by Banco Sabadell Foundation and funding from the Valencian Government (Conselleria d’Innovació, Indústria, Comerç i Turisme, Direcció General para el Avance de la Sociedad Digital) by virtue of a 2023 grant agreement (convenio singular 2023).

[‡]<https://www.deel.ai/>

References

- [1] Chris Olah, Alexander Mordvintsev, and Ludwig Schubert. Feature visualization. *Distill*, 2(11):e7, 2017.
- [2] Finale Doshi-Velez and Been Kim. Towards a rigorous science of interpretable machine learning. *ArXiv e-print*, 2017.
- [3] Alon Jacovi, Ana Marasović, Tim Miller, and Yoav Goldberg. Formalizing trust in artificial intelligence: Prerequisites, causes and goals of human trust in ai. In *Proceedings of the 2021 ACM conference on fairness, accountability, and transparency*, pages 624–635, 2021.
- [4] Karen Simonyan, Andrea Vedaldi, and Andrew Zisserman. Deep inside convolutional networks: Visualising image classification models and saliency maps. In *Workshop Proceedings of the International Conference on Learning Representations (ICLR)*, 2014.
- [5] Daniel Smilkov, Nikhil Thorat, Been Kim, Fernanda Viégas, and Martin Wattenberg. Smoothgrad: removing noise by adding noise. In *Workshop on Visualization for Deep Learning, Proceedings of the International Conference on Machine Learning (ICML)*, 2017.
- [6] Ramprasaath R Selvaraju, Michael Cogswell, Abhishek Das, Ramakrishna Vedantam, Devi Parikh, and Dhruv Batra. Grad-cam: Visual explanations from deep networks via gradient-based localization. In *Proceedings of the IEEE international conference on computer vision*, pages 618–626, 2017.
- [7] Thomas Fel, Remi Cadene, Mathieu Chalvidal, Matthieu Cord, David Vigouroux, and Thomas Serre. Look at the variance! efficient black-box explanations with sobol-based sensitivity analysis. In *Advances in Neural Information Processing Systems (NeurIPS)*, 2021.
- [8] Paul Novello, Thomas Fel, and David Vigouroux. Making sense of dependence: Efficient black-box explanations using dependence measure. In *Advances in Neural Information Processing Systems (NeurIPS)*, 2022.
- [9] Mukund Sundararajan, Ankur Taly, and Qiqi Yan. Axiomatic attribution for deep networks. In *Proceedings of the International Conference on Machine Learning (ICML)*, 2017.
- [10] Matthew D Zeiler and Rob Fergus. Visualizing and understanding convolutional networks. In *Computer Vision—ECCV 2014: 13th European Conference, Zurich, Switzerland, September 6–12, 2014, Proceedings, Part I 13*, pages 818–833. Springer, 2014.
- [11] Avanti Shrikumar, Peyton Greenside, and Anshul Kundaje. Learning important features through propagating activation differences. In *Proceedings of the International Conference on Machine Learning (ICML)*, 2017.
- [12] Ruth C. Fong and Andrea Vedaldi. Interpretable explanations of black boxes by meaningful perturbation. In *Proceedings of the IEEE International Conference on Computer Vision (ICCV)*, 2017.
- [13] Mara Graziani, Iam Palatnik de Sousa, Marley MBR Vellasco, Eduardo Costa da Silva, Henning Müller, and Vincent Andrearczyk. Sharpening local interpretable model-agnostic explanations for histopathology: improved understandability and reliability. In *Medical Image Computing and Computer Assisted Intervention (MICCAI)*. Springer, 2021.
- [14] Vitali Petsiuk, Abir Das, and Kate Saenko. Rise: Randomized input sampling for explanation of black-box models. In *Proceedings of the British Machine Vision Conference (BMVC)*, 2018.
- [15] Thomas Fel, Melanie Ducoffe, David Vigouroux, Remi Cadene, Mikael Capelle, Claire Nicodeme, and Thomas Serre. Don’t lie to me! robust and efficient explainability with verified perturbation analysis. *Proceedings of the IEEE Conference on Computer Vision and Pattern Recognition (CVPR)*, 2023.
- [16] Marouane El Idrissi, Nicolas Bousquet, Fabrice Gamboa, Bertrand Iooss, and Jean-Michel Loubes. On the coalitional decomposition of parameters of interest, 2023.
- [17] Julien Colin, Thomas Fel, Rémi Cadène, and Thomas Serre. What i cannot predict, i do not understand: A human-centered evaluation framework for explainability methods. *Advances in Neural Information Processing Systems (NeurIPS)*, 2021.
- [18] Sunnie S. Y. Kim, Nicole Meister, Vikram V. Ramaswamy, Ruth Fong, and Olga Russakovsky. HIVE: Evaluating the human interpretability of visual explanations. In *Proceedings of the IEEE European Conference on Computer Vision (ECCV)*, 2022.

- [19] Giang Nguyen, Daeyoung Kim, and Anh Nguyen. The effectiveness of feature attribution methods and its correlation with automatic evaluation scores. *Advances in Neural Information Processing Systems (NeurIPS)*, 2021.
- [20] Anh Nguyen, Jason Yosinski, and Jeff Clune. Understanding neural networks via feature visualization: A survey. *Explainable AI: interpreting, explaining and visualizing deep learning*, pages 55–76, 2019.
- [21] Leon Sixt, Martin Schuessler, Oana-Iuliana Popescu, Philipp Weiß, and Tim Landgraf. Do users benefit from interpretable vision? a user study, baseline, and dataset. *Proceedings of the International Conference on Learning Representations (ICLR)*, 2022.
- [22] Peter Hase and Mohit Bansal. Evaluating explainable ai: Which algorithmic explanations help users predict model behavior? *Proceedings of the Annual Meeting of the Association for Computational Linguistics (ACL Short Papers)*, 2020.
- [23] Leon Sixt, Maximilian Granz, and Tim Landgraf. When explanations lie: Why many modified by attributions fail. In *Proceedings of the International Conference on Machine Learning (ICML)*, 2020.
- [24] Julius Adebayo, Justin Gilmer, Michael Muelly, Ian Goodfellow, Moritz Hardt, and Been Kim. Sanity checks for saliency maps. In *Advances in Neural Information Processing Systems (NIPS)*, 2018.
- [25] Dylan Slack, Anna Hilgard, Sameer Singh, and Himabindu Lakkaraju. Reliable post hoc explanations: Modeling uncertainty in explainability. *Advances in Neural Information Processing Systems (NeurIPS)*, 34, 2021.
- [26] Sukrut Rao, Moritz Böhle, and Bernt Schiele. Towards better understanding attribution methods. In *Proceedings of the IEEE Conference on Computer Vision and Pattern Recognition (CVPR)*, 2022.
- [27] Christian Szegedy, Wojciech Zaremba, Ilya Sutskever, Joan Bruna, Dumitru Erhan, Ian Goodfellow, and Rob Fergus. Intriguing properties of neural networks. *arXiv preprint arXiv:1312.6199*, 2013.
- [28] Aravindh Mahendran and Andrea Vedaldi. Understanding deep image representations by inverting them. In *Proceedings of the IEEE conference on computer vision and pattern recognition*, pages 5188–5196, 2015.
- [29] Anh Nguyen, Jason Yosinski, and Jeff Clune. Deep neural networks are easily fooled: High confidence predictions for unrecognizable images. In *Proceedings of the IEEE conference on computer vision and pattern recognition*, pages 427–436, 2015.
- [30] Mike Tyka. Class visualization with bilateral filters. 2016. URL: <https://mtyka.github.io/deepdream/2016/02/05/bilateral-class-vis.html>, 2(3), 2016.
- [31] M. Øygard Audun. Visualizing googlenet classes. URL: <https://www.auduno.com/2015/07/29/visualizing-googlenet-classes/>, 2(3), 2015.
- [32] Dimitris Tsipras, Shibani Santurkar, Logan Engstrom, Alexander Turner, and Aleksander Madry. Robustness may be at odds with accuracy. *arXiv preprint arXiv:1805.12152*, 2018.
- [33] Shibani Santurkar, Andrew Ilyas, Dimitris Tsipras, Logan Engstrom, Brandon Tran, and Aleksander Madry. Image synthesis with a single (robust) classifier. *Advances in Neural Information Processing Systems*, 32, 2019.
- [34] Logan Engstrom, Andrew Ilyas, Shibani Santurkar, Dimitris Tsipras, Brandon Tran, and Aleksander Madry. Adversarial robustness as a prior for learned representations. *arXiv preprint arXiv:1906.00945*, 2019.
- [35] Alexander Mordvintsev, Christopher Olah, and Mike Tyka. Inceptionism: Going deeper into neural networks. <https://blog.research.google/2015/06/inceptionism-going-deeper-into-neural.html?m=1>, 2015.
- [36] Amin Ghiasi, Hamid Kazemi, Steven Reich, Chen Zhu, Micah Goldblum, and Tom Goldstein. Plug-in inversion: Model-agnostic inversion for vision with data augmentations. *Proceedings of the International Conference on Machine Learning (ICML)*, 2021.
- [37] Amin Ghiasi, Hamid Kazemi, Eitan Borgnia, Steven Reich, Manli Shu, Micah Goldblum, Andrew Gordon Wilson, and Tom Goldstein. What do vision transformers learn? a visual exploration. *preprint*, 2022.
- [38] Donglai Wei, Bolei Zhou, Antonio Torralba, and William Freeman. Understanding intra-class knowledge inside cnn. *arXiv preprint arXiv:1507.02379*, 2015.

- [39] Anh Nguyen, Jason Yosinski, and Jeff Clune. Multifaceted feature visualization: Uncovering the different types of features learned by each neuron in deep neural networks. *Visualization for Deep Learning workshop, Proceedings of the International Conference on Machine Learning (ICML)*, 2016.
- [40] Anh Nguyen, Alexey Dosovitskiy, Jason Yosinski, Thomas Brox, and Jeff Clune. Synthesizing the preferred inputs for neurons in neural networks via deep generator networks. *Advances in neural information processing systems*, 29, 2016.
- [41] Anh Nguyen, Jeff Clune, Yoshua Bengio, Alexey Dosovitskiy, and Jason Yosinski. Plug & play generative networks: Conditional iterative generation of images in latent space. In *Proceedings of the IEEE conference on computer vision and pattern recognition*, pages 4467–4477, 2017.
- [42] Kaiming He, Xiangyu Zhang, Shaoqing Ren, and Jian Sun. Deep residual learning for image recognition. In *Proceedings of the IEEE Conference on Computer Vision and Pattern Recognition (CVPR)*, 2016.
- [43] A Dosovitskiy, L Beyer, Alexander Kolesnikov, Dirk Weissenborn, Xiaohua Zhai, Thomas Unterthiner, M Dehghani, Matthias Minderer, G Heigold, S Gelly, Jakob Uszkoreit, and N Houlsby. An image is worth 16x16 words: Transformers for image recognition at scale. *ICLR*, 2021.
- [44] Alan V Oppenheim and Jae S Lim. The importance of phase in signals. *Proceedings of the IEEE*, 69(5):529–541, 1981.
- [45] Terry Caelli and Paul Bevan. Visual sensitivity to two-dimensional spatial phase. *JOSA*, 72(10):1375–1381, 1982.
- [46] Nathalie Guyader, Alan Chauvin, Carole Peyrin, Jeanny Hérault, and Christian Marendaz. Image phase or amplitude? rapid scene categorization is an amplitude-based process. *Comptes Rendus Biologies*, 327(4):313–318, 2004.
- [47] Olivier R Joubert, Guillaume A Rousselet, Michele Fabre-Thorpe, and Denis Fize. Rapid visual categorization of natural scene contexts with equalized amplitude spectrum and increasing phase noise. *Journal of Vision*, 9(1):2–2, 2009.
- [48] Evgeny Gladilin and Roland Eils. On the role of spatial phase and phase correlation in vision, illusion, and cognition. *Frontiers in Computational Neuroscience*, 9:45, 2015.
- [49] Lucas Beyer, Pavel Izmailov, Alexander Kolesnikov, Mathilde Caron, Simon Kornblith, Xiaohua Zhai, Matthias Minderer, Michael Tschannen, Ibrahim Alabdulmohsin, and Filip Pavetic. Flexivit: One model for all patch sizes. *arXiv preprint arXiv:2212.08013*, 2022.
- [50] Thomas Fel, Agustin Picard, Louis Bethune, Thibaut Boissin, David Vigouroux, Julien Colin, Rémi Cadène, and Thomas Serre. Craft: Concept recursive activation factorization for explainability. *Proceedings of the IEEE Conference on Computer Vision and Pattern Recognition (CVPR)*, 2022.
- [51] Dumitru Erhan, Yoshua Bengio, Aaron Courville, and Pascal Vincent. Visualizing higher-layer features of a deep network. *University of Montreal*, 1341(3):1, 2009.
- [52] Guangrun Wang and Philip HS Torr. Traditional classification neural networks are good generators: They are competitive with dpms and gans. *arXiv preprint arXiv:2211.14794*, 2022.
- [53] Alexander Mordvintsev, Nicola Pezzotti, Ludwig Schubert, and Chris Olah. Differentiable image parameterizations. *Distill*, 2018.
- [54] Judy Borowski, Roland S Zimmermann, Judith Schepers, Robert Geirhos, Thomas SA Wallis, Matthias Bethge, and Wieland Brendel. Exemplary natural images explain cnn activations better than state-of-the-art feature visualization. *arXiv preprint arXiv:2010.12606*, 2020.
- [55] Victor Boutin, Thomas Fel, Lakshya Singhal, Rishav Mukherji, Akash Nagaraj, Julien Colin, and Thomas Serre. Diffusion models as artists: Are we closing the gap between humans and machines? *arXiv preprint arXiv:2301.11722*, 2023.
- [56] Yiyu Sun, Yifei Ming, Xiaojin Zhu, and Yixuan Li. Out-of-distribution detection with deep nearest neighbors. In *International Conference on Machine Learning*, pages 20827–20840. PMLR, 2022.
- [57] Andrew G Howard, Menglong Zhu, Bo Chen, Dmitry Kalenichenko, Weijun Wang, Tobias Weyand, Marco Andreetto, and Hartwig Adam. Mobilenets: Efficient convolutional neural networks for mobile vision applications. *arXiv preprint arXiv:1704.04861*, 2017.

- [58] Karen Simonyan and Andrew Zisserman. Very deep convolutional networks for large-scale image recognition. *arXiv preprint arXiv:1409.1556*, 2014.
- [59] François Chollet. Xception: Deep learning with depthwise separable convolutions. In *Proceedings of the IEEE conference on computer vision and pattern recognition*, pages 1251–1258, 2017.
- [60] Mingxing Tan and Quoc Le. Efficientnet: Rethinking model scaling for convolutional neural networks. In *International conference on machine learning*, pages 6105–6114. PMLR, 2019.
- [61] Zhuang Liu, Hanzi Mao, Chao-Yuan Wu, Christoph Feichtenhofer, Trevor Darrell, and Saining Xie. A convnet for the 2020s. In *Proceedings of the IEEE/CVF Conference on Computer Vision and Pattern Recognition*, pages 11976–11986, 2022.
- [62] Gao Huang, Zhuang Liu, Laurens Van Der Maaten, and Kilian Q Weinberger. Densely connected convolutional networks. In *Proceedings of the IEEE conference on computer vision and pattern recognition*, pages 4700–4708, 2017.
- [63] Alexander Kolesnikov, Lucas Beyer, Xiaohua Zhai, Joan Puigcerver, Jessica Yung, Sylvain Gelly, and Neil Houlsby. Big transfer (bit): General visual representation learning. In *Computer Vision – ECCV 2020: 16th European Conference, Glasgow, UK, August 23–28, 2020, Proceedings, Part V*, page 491–507, Berlin, Heidelberg, 2020. Springer-Verlag.
- [64] Kaiming He, Xiangyu Zhang, Shaoqing Ren, and Jian Sun. Identity mappings in deep residual networks. In *Computer Vision–ECCV 2016: 14th European Conference, Amsterdam, The Netherlands, October 11–14, 2016, Proceedings, Part IV 14*, pages 630–645. Springer, 2016.
- [65] Timothy Dozat. Incorporating nesterov momentum into adam. *Proceedings of the International Conference on Learning Representations (ICLR)*, 2016.
- [66] Thomas Fel, Lucas Hervier, David Vigouroux, Antonin Poche, Justin Plakoo, Remi Cadene, Mathieu Chalvidal, Julien Colin, Thibaut Boissin, Louis Bethune, Agustin Picard, Claire Nicodeme, Laurent Gardes, Gregory Flandin, and Thomas Serre. Xplique: A deep learning explainability toolbox. *Workshop on Explainable Artificial Intelligence for Computer Vision (CVPR)*, 2022.
- [67] Roland S Zimmermann, Judy Borowski, Robert Geirhos, Matthias Bethge, Thomas Wallis, and Wieland Brendel. How well do feature visualizations support causal understanding of cnn activations? *Advances in Neural Information Processing Systems*, 34:11730–11744, 2021.
- [68] Amirata Ghorbani, James Wexler, James Y Zou, and Been Kim. Towards automatic concept-based explanations. *Advances in Neural Information Processing Systems*, 32, 2019.
- [69] Robert Geirhos, Roland S. Zimmermann, Blair Bilodeau, Wieland Brendel, and Been Kim. Don’t trust your eyes: on the (un)reliability of feature visualizations, 2023.
- [70] J. Deng, W. Dong, R. Socher, L.-J. Li, K. Li, and L. Fei-Fei. ImageNet: A Large-Scale Hierarchical Image Database. In *Proceedings of the IEEE Conference on Computer Vision and Pattern Recognition (CVPR)*, 2009.

A Additional results	16
A.1 Logit and Internal State Visualization	17
A.2 Feature Inversion	19
B Screenshots from the website	19
C Human psychophysical study	22

A Additional results

In this section, we provide additional results for logit and internal feature visualizations, and feature inversion.

For all of the following visualizations, we used the same parameters as in the main paper. For the feature visualizations derived from Olah *et al.* [1], we used all 10 transformations set from the Lucid library[§]. For **MACO**, τ only consists of two transformations; first we add uniform noise $\delta \sim \mathcal{U}([-0.1, 0.1])^{W \times H}$ and crops and resized the image with a crop size drawn from the normal distribution $\mathcal{N}(0.25, 0.1)$, which corresponds on average to 25% of the image. We used the NAdam optimizer [65] with a $lr = 1.0$ and $N = 256$ optimization steps. Finally, we used the implementation of [1] and CBR which are available in the Xplique library [66][¶] which is based on Lucid.

[§]<https://github.com/tensorflow/lucid>
[¶]<https://github.com/deel-ai/xplique>

A.1 Logit and Internal State Visualization

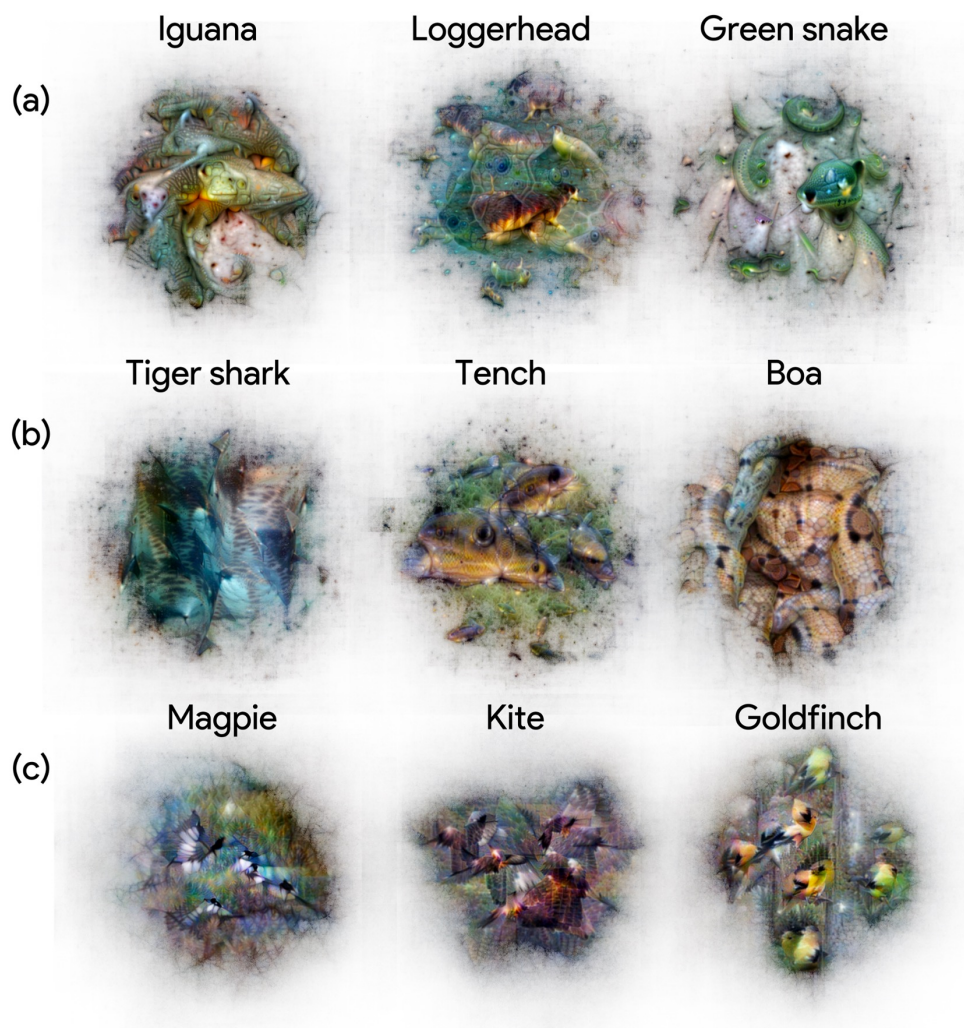


Figure S1: **Feature visualizations on FlexiViT, ViT and ResNet50.** We compare the feature visualizations from **MACO** generated for (a) FlexiViT, (b) ViT and (c) ResNet50 on a set of different classes from ImageNet. We observe that the visualizations get more abstract as the complexity of the model increases.

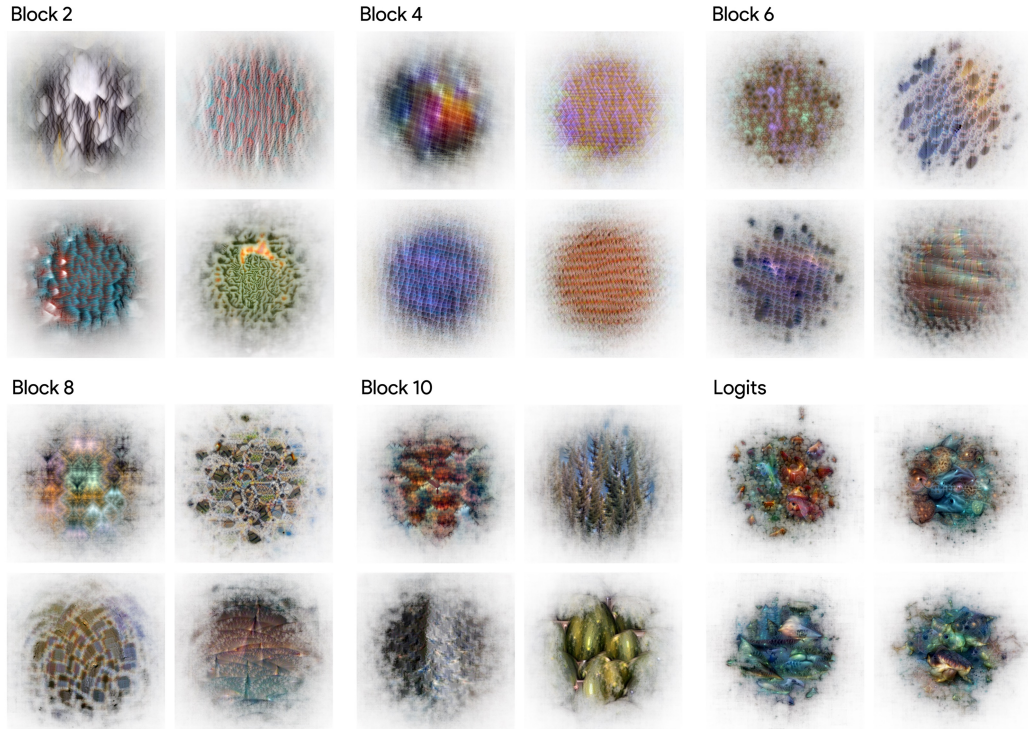


Figure S2: **Logits and internal representation of a ViT.** Using **MACO**, we maximize the activations of specific channels in different blocks of a ViT, as well as the logits for 4 different classes.



Figure S3: **Hue invariance.** Through feature visualization, we are able to determine the presence of hue invariance on our pre-trained ViT model manifesting itself through phantom objects in them. This can be explained the data-augmentation that is typically employed for training these models.

A.2 Feature Inversion

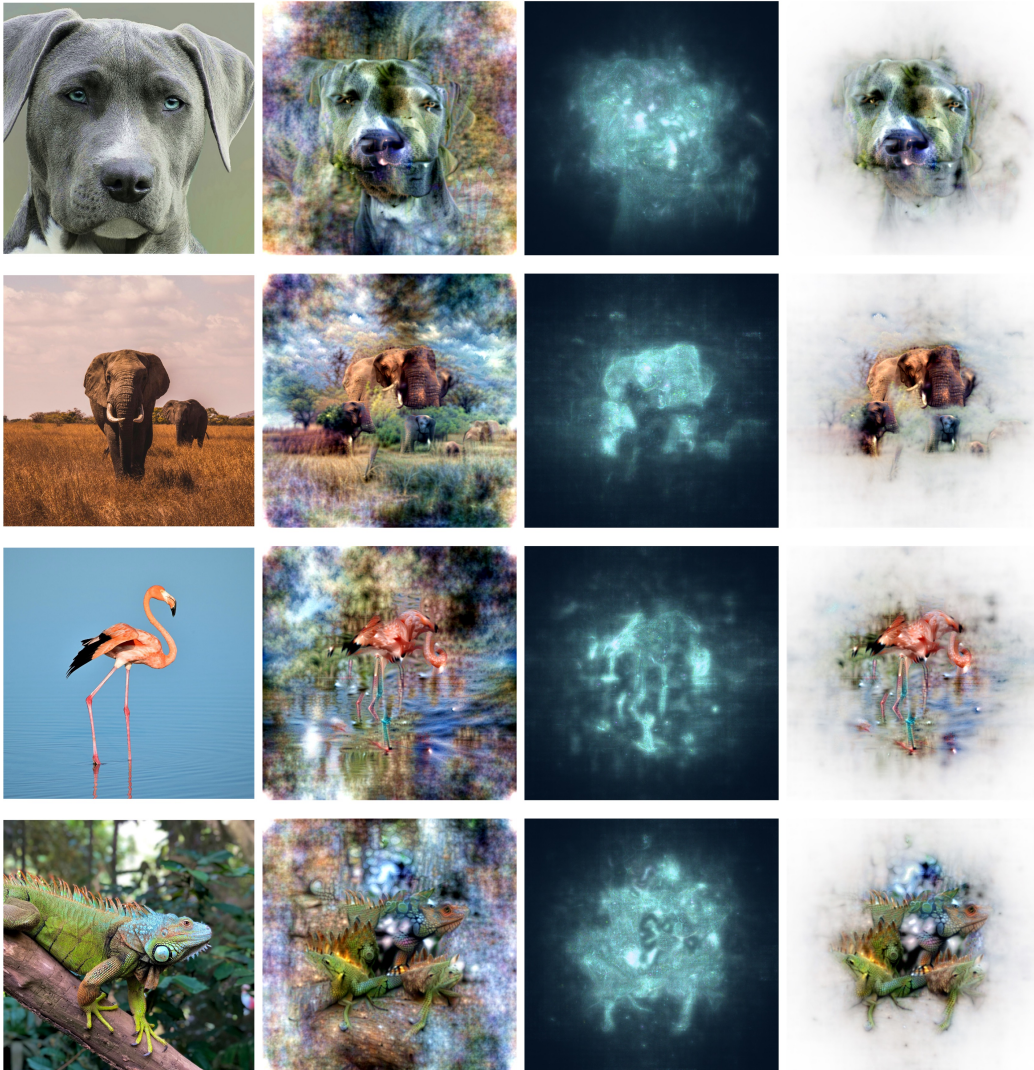


Figure S4: **Feature inversion and Attribution-based transparency.** We performed feature inversion on the images on the first column to obtain the visualizations (without transparency) on the second column. During the optimization procedure, we saved the intensity of the changes to the image in pixel space, which we showcase on the third column, we used this information to assign a transparency value, as exhibited in the final column.

B Screenshots from the website

For our website, we picked a ResNet50V2 that had been pre-trained on ImageNet [70] and applied CRAFT [50] to reveal the concepts that are driving its predictions for each class. CRAFT is a state-of-the-art, concept-based explainability technique that, through NMF matrix decompositions, allows us to factorize the networks activations into interpretable concepts. Furthermore, using Sobol indices and implicit differentiation, we can measure the importance of each concept, and trace its presence back to and locate it in the input image.

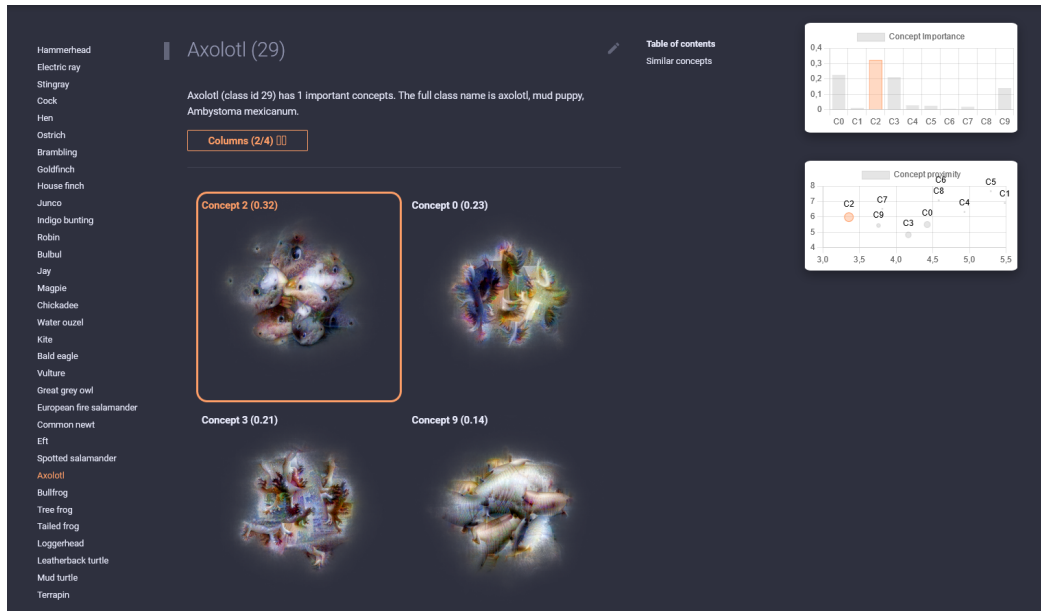


Figure S5: **Overview of a class explanation.** Screenshot of the first glimpse of the explanations for the class *axolotl*. We display the concept visualizations by order of importance (the most important concepts first), with a bar plot of the importance scores and a plot of their similarity.

In particular, we applied this technique to explain all the classes in ImageNet, and used **MACO** to generate visualizations that maximize the angle of superposition with each direction in the network’s activation space (i.e. each concept). We also plot each of the concepts’ global importance, as well as the similarities between concepts of the same class. For each class, we first showcase the most important concepts with their respective visualizations (see Fig. S5 and Fig. S6), and by clicking on them, we exhibit the crops that align the most with the concept (see Fig. S7). This allows us to diminish the effect of potential confirmation bias by providing two different approaches to understanding what the model has encoded in that concept.

Finally, we have also computed the similarity between concepts of different classes and display the closest (see Fig. S8). This feature can help better understand erroneous predictions, as the model may sometimes leverage similar concepts of different classes to classify.

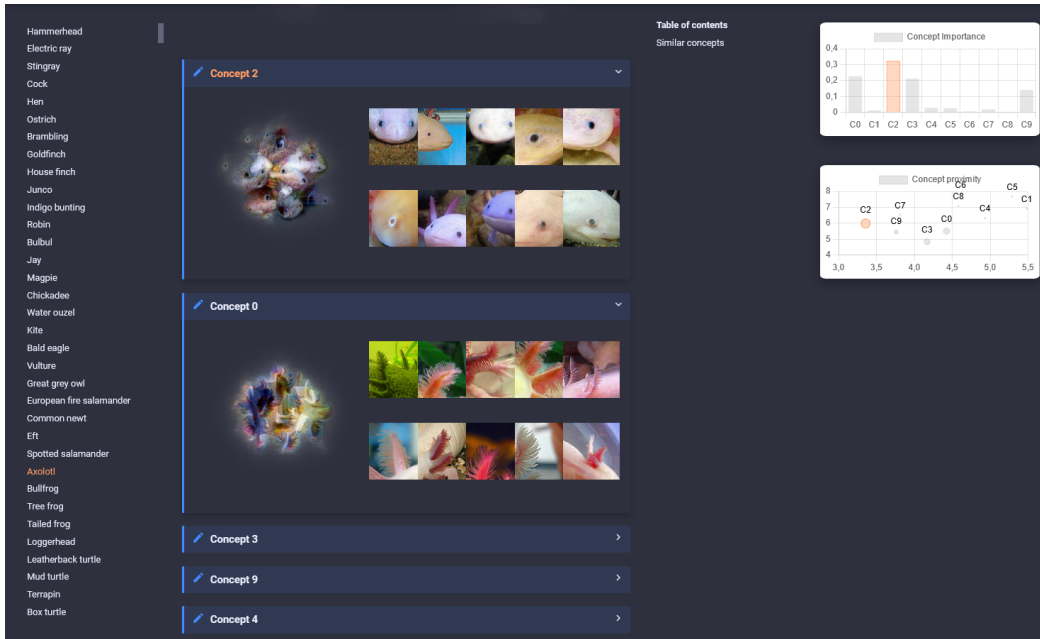


Figure S6: **Most representative crops.** If we scroll down, we get access to the crops that represent the most each of the concepts alongside the visualizations. By representing the concepts through two different approaches side by side, we reduce the effect of confirmation bias.

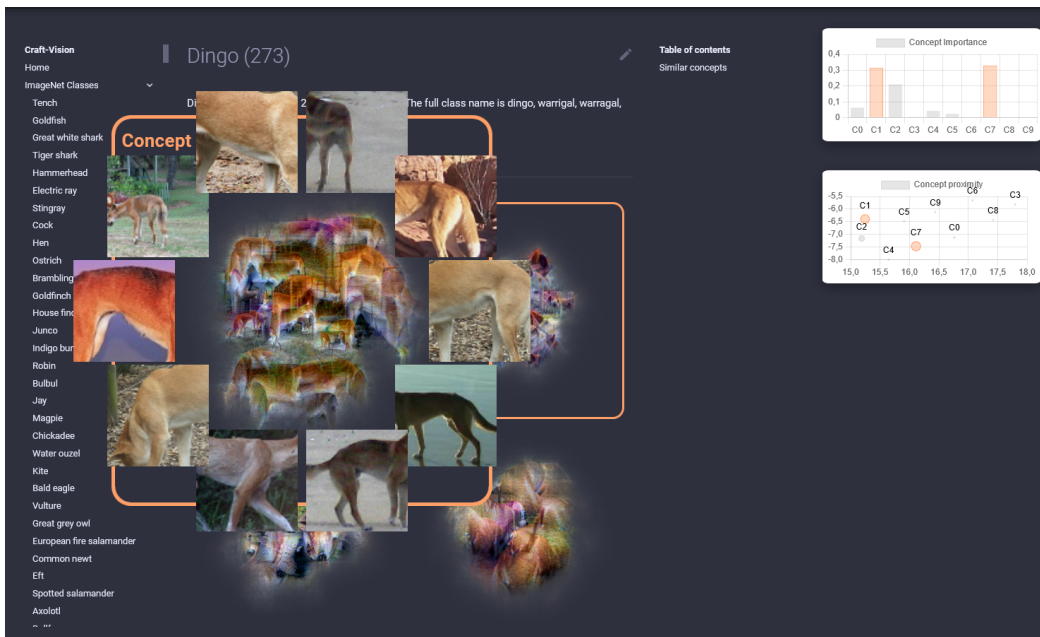


Figure S7: **Revealing the crops.** On the first overview, it is also possible to click on each concept to reveal the most representative crops.

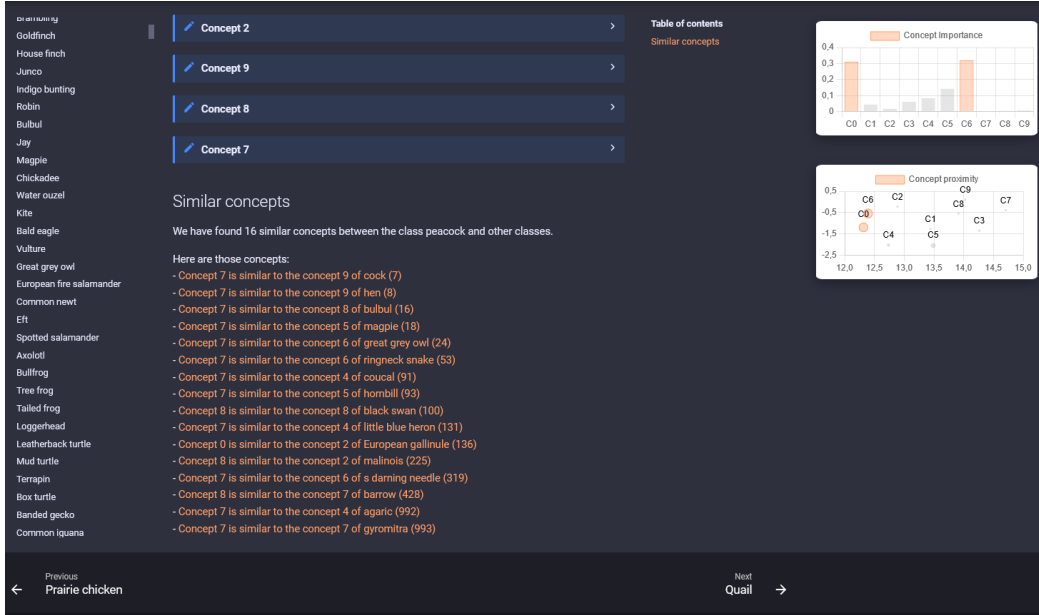


Figure S8: **Inter-class concept similarity.** Scrolling further down, we also present the concepts from other classes that are the most similar to those of the current class. This can help better understand erroneous predictions, as the model may sometimes leverage similar concepts of different classes to classify.

C Human psychophysical study

To evaluate **MACO**'s ability to improve humans' causal understanding of a CNN's activations, we conducted a psychophysical study closely following the paradigm introduced in [67]. In this paradigm, participants are asked to predict which of two query inputs would be favored by the model (i.e., maximally activate a given unit), based on example "favorite" inputs serving as a reference (i.e., feature visualizations for that unit). The two queries are based on the same natural image, but differ in the location of an occluder which hides part of the image from the model.

Participants. We recruited a total of 191 participants for our online psychophysics study using Prolific (www.prolific.com) [September 2023]. As compensation for their time (roughly 7 minutes), participants were paid 1.4\$. Of those who chose to disclose their age, the average age was 39 years old ($SD = 13$). Ninety participants were men, 86 women, 8 non-binary and 7 chose not to disclose their gender. The data of 17 participants was excluded from further analyses because they performed significantly below chance ($p < .05$, one-tailed).

Design. Participants were randomly assigned to one of four Visualization conditions: Olah [1], **MACO** with mask, **MACO** without mask, or a control condition in which no visualizations were provided. Furthermore, we varied Network (VGG16, ResNet50, ViT) as a within-subjects variable. The specific units whose features to visualize were taken from the output layer, meaning they represented concrete classes. The classes were: Nile crocodile, peacock, Kerry Blue Terrier, Giant Schnauzer, Bernese Mountain Dog, ground beetle, ringlet, llama, apiary, cowboy boot, slip-on shoe, mask, computer mouse, muzzle, obelisk, ruler, hot dog, broccoli, and mushroom. For every class, we included three natural images to serve as the source image for the query pairs. This way, a single participant would see all 19 classes crossed with all 3 networks, without seeing the same natural image more than once (which image was presented for which network was randomized across participants). The main experiment thus consisted of 57 trials, with a fully randomized trial order.

Stimuli. The stimuli for this study included 171 ((4-1)x3x19) reference stimuli, each displaying a 2x2 grid of feature visualizations, generated using the respective visualization method. The query pairs were created from each of the 57 (19x3) source images by placing a square occluder on them.

In one member of the pair, the occludor was placed such that it minimized the activation of the unit. In the other member of the pair, the occludor was placed on an object of a different class in the same image or a different part of the same object. Here, we deviated somewhat from the query generation in [67], where the latter occludor was placed where it maximized the activation of the unit. However, we observed that this often resulted in the occludor being on the background, making the task trivial. Indeed, a pilot study ($N = 42$) we ran with such occludor placement showed that even the participants in the control condition were on average correct in 83% of the trials.

Task and procedure. The protocol was approved by the University IRB and was carried out in accordance with the provisions of the World Medical Association Declaration of Helsinki. Participants were redirected to our online study through Prolific and first saw a page explaining the general purpose and procedure of the study (Fig. S9). Next, they were presented with a form outlining their rights as a participant and actively had to click “I agree” in order to give their consent. More detailed instructions were given on the next page (Fig. S10, Fig. S11). Participants were instructed to answer the following question on every trial: “Which of the two query images is more favored by the machine?”. The two query images were presented on the right-hand side of the screen. The feature visualizations were displayed on the left-hand side of the screen (Fig. S12). In the control condition, the left-hand side remained blank (Fig. S13). Participants could make their response by clicking on the radio button below the respective query image. They first completed a practice phase, consisting of six trials covering two additional classes, before moving on to the main experiment. For the practice trials, they received feedback in the form of a green (red) frame appearing around their selected query image if they were correct (incorrect). No such feedback was given during the main experiment.

Analyses and results. We analyzed the data through a logistic mixed-effects regression analysis, with trial accuracy (1 vs. 0) as the dependent variable. The random-effects structure included a by-participant random intercept and by-class random intercept. We compared two regression models, both of which had Visualization and Network as a fixed effect, but only one also fitted an interaction term between the two. Based on the Akaike Information Criterion (AIC), the former, less complex model was selected ($AIC = 11481$ vs. 11482). Using this model, we then analyzed all pairwise contrasts between the levels of the Visualization variable. We found that the logodds of choosing the correct query were overall significantly higher in both **MACO** conditions compared to the control condition: $\beta_{\text{MACO Mask}} - \beta_{\text{Control}} = 0.69$, $SE = 0.13$, $z = 5.38$, $p < .0001$; $\beta_{\text{MACO NoMask}} - \beta_{\text{Control}} = 0.92$, $SE = 0.13$, $z = 7.07$, $p < .0001$. Moreover, **MACO** visualizations helped more than Olah visualizations: $\beta_{\text{MACO Mask}} - \beta_{\text{Olah}} = 0.43$, $SE = 0.13$, $z = 3.31$, $p = .005$; $\beta_{\text{MACO NoMask}} - \beta_{\text{Olah}} = 0.66$, $SE = 0.13$, $z = 4.99$, $p < .0001$. No other contrasts were statistically significant (at a level of $p < .05$). P -values were adjusted for multiple comparisons with the Tukey method. Finally, we also examined the pairwise contrasts for the Network variable. We found that ViT was the hardest model to interpret overall: $\beta_{\text{ResNet50}} - \beta_{\text{ViT}} = 0.49$, $SE = 0.06$, $z = 8.65$, $p < .0001$; $\beta_{\text{VGG16}} - \beta_{\text{ViT}} = 0.35$, $SE = 0.06$, $z = 6.38$, $p < .0001$. There was only marginally significant evidence that participants could better predict ResNet50’s behavior in this task than VGG16: $\beta_{\text{ResNet50}} - \beta_{\text{VGG16}} = 0.13$, $SE = 0.06$, $z = 2.30$, $p = 0.056$.

Taken together, these results suggest that **MACO** indeed helps humans causally understand a CNN’s activations and that it outperforms Olah’s method [1] on this criterion.

AI's Favorite Images

Contacts: lore_goetschalckx@brown.edu · julien_colin@brown.edu

Welcome

This is a computational neuroscience study looking to discover how artificial intelligence (AI) "thinks". Specifically, we are interested in machines trained to recognize images. You will be asked to complete a 6-9 min task. The task consists of several trials. On each trial, you will be shown images and asked to respond by clicking the mouse.

The question you will have to respond to is:

Which of the two images presented to you is more favored by the machine?

The machines we are considering in this study are trained to recognize images. Participants are randomly assigned to different groups. Depending on the group you are in, you might see examples of a couple of the machine's favorite images to help you with your task. These examples are computer-generated and might look a little funky.

More detailed instructions will follow, but first please take notice of the prerequisites below.

Prerequisites

1. You are working on a desktop or laptop, not on a phone or a tablet.
2. You have normal or corrected-to-normal vision.

Please make a participation code using the first letter of your mother's name, the first letter of your father's name, first letter of your favorite hobby, and the last digit of your house number (e.g., PCB0). Please enter your unique code before clicking Continue.

On the next page, we will first ask you for your consent to participate in this study.

Continue

This task is part of a scientific research project of Brown University. Your decision to participate is voluntary. There is no way for us to identify you. The only information we will have is: your responses, your participation code, your age and gender (should you choose to disclose that), and the time at which you started and quit the task. The results of the research may be presented at scientific meetings or published in scientific journals. Choosing to participate indicates that you agree to do this voluntarily. If you have questions about this research, please contact Lore Goetschalckx at lore_goetschalckx@brown.edu and Julien Colin at julien_colin@brown.edu.

Figure S9: Welcome page. This is a screenshot of the first page participants saw when entering our online psychophysics study.

Instructions

You are in the group who will see examples of a machine's favorite images.

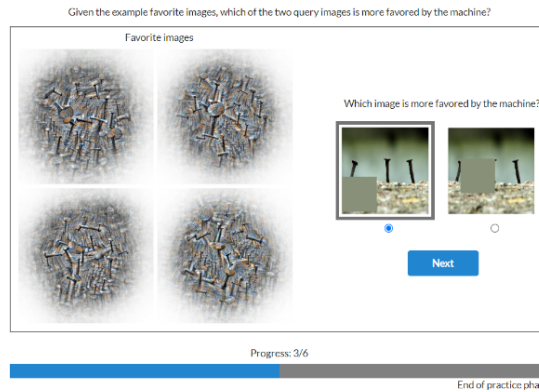
On each trial, the screen will be divided into two sections:

- LEFT: A group of example images. These are the favorite images of a machine. Usually, these images share at least one common aspect.
- RIGHT: Two query images. In each query image, a square has been placed to cover part of the image. This part is hidden to the machine.

The question you have to answer is always the following: **Which of the two query images is more favored by the machine?** In other words, in which image do you still see the common aspect of the favorite images?

Answer by clicking on the button below the image that you believe to be favored by the machine. A grey frame will appear around your chosen image.

The image below shows you what a single trial will look like.



Before starting the main task, there will be several practice trials such that you can familiarize yourself with the task.

Continue

Figure S10: **Instructions page.** After providing informed consent, participants in our online psychophysics task received more detailed instructions, as shown here.

Instructions

You are in the group who won't see examples of a machine's favorite images. Don't worry. That's not bad. We're merely interested in your sincere responses to the task.

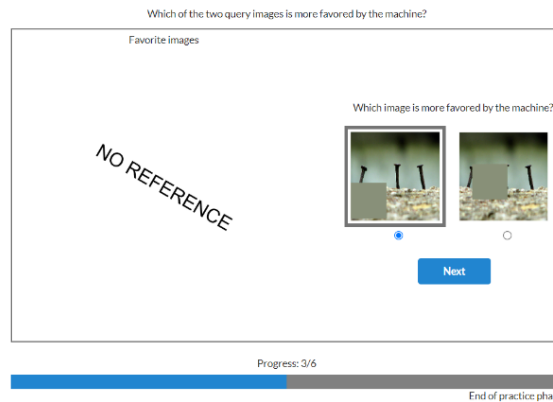
On each trial, the screen will be divided into two sections:

- LEFT: There won't be any images shown on this side.
- RIGHT: Two query images. In each query image, a square has been placed to cover part of the image. This part is hidden to the machine.

The question you have to answer is always the following: **Which of the two query images is more favored by the machine?**

Answer by clicking on the button below the image that you believe to be favored by the machine. A grey frame will appear around your chosen image.

The image below shows you what a single trial will look like.



Before starting the main task, there will be several practice trials such that you can familiarize yourself with the task.

[Continue](#)

Figure S11: Instructions page for control condition. After providing informed consent, participants in our online psychophysics task received more detailed instructions, as shown here. If they were randomly assigned to the control condition, they were informed that they would not see examples of the machine's favorite images.

's Favorite Images

Contacts: lore_goetschalckx@brown.edu - julien_colin@brown.edu

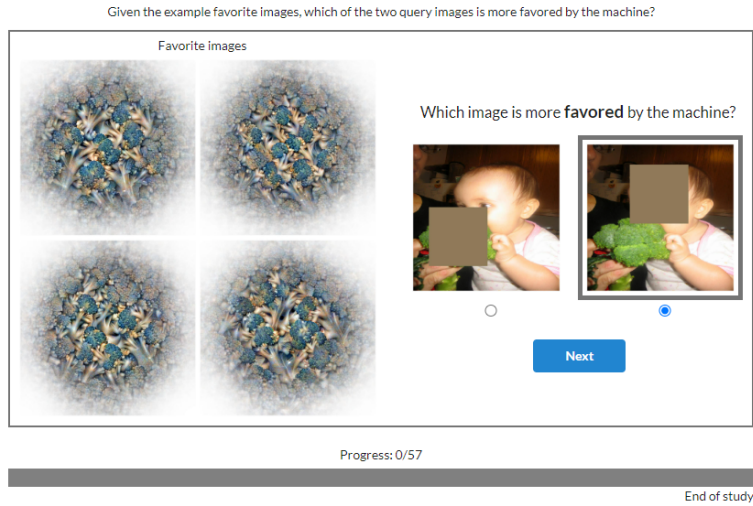


Figure S12: **Example trial.** On every trial of our psychophysics study, participants were asked to select which of two query images would be favored by the machine. They were shown examples of the machine's favorite inputs (i.e., feature visualizations) on the left side of the screen.

's Favorite Images

Contacts: lore_goetschalckx@brown.edu - julien_colin@brown.edu

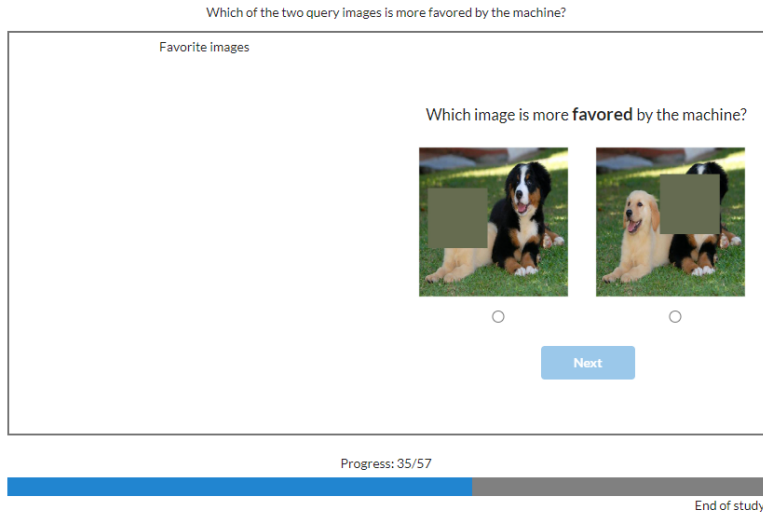


Figure S13: **Example trial in the control condition.** On every trial of our psychophysics study, participants were asked to select which of two query images would be favored by the machine. In the control condition, they were not shown examples of the machine's favorite inputs and the left side of the screen remained empty.